nature neuroscience

Action potential generation requires a high sodium channel density in the axon initial segment

Maarten H P Kole[1], Susanne U Ilschner[1], Björn M Kampa[1,4], Stephen R Williams[1,2], Peter C Ruben[1,3] & Greg J Stuart[1]

The axon initial segment (AIS) is a specialized region in neurons where action potentials are initiated. It is commonly assumed that this process requires a high density of voltage-gated sodium (Na^+) channels. Paradoxically, the results of patch-clamp studies suggest that the Na^+ channel density at the AIS is similar to that at the soma and proximal dendrites. Here we provide data obtained by antibody staining, whole-cell voltage-clamp and Na^+ imaging, together with modeling, which indicate that the Na^+ channel density at the AIS of cortical pyramidal neurons is ~50 times that in the proximal dendrites. Anchoring of Na^+ channels to the cytoskeleton can explain this discrepancy, as disruption of the actin cytoskeleton increased the Na^+ current measured in patches from the AIS. Computational models required a high Na^+ channel density (~2,500 pS μm^{-2}) at the AIS to account for observations on action potential generation and backpropagation. In conclusion, action potential generation requires a high Na^+ channel density at the AIS, which is maintained by tight anchoring to the actin cytoskeleton.

Action potentials are the primary means of fast communication between neurons. Work dating back to the mid-1950s, using sharp microelectrode recordings from the somata of cat spinal motoneurons, indicated that action potentials are initiated in the initial segment of the axon[1–3]. Similar conclusions were subsequently drawn from studies of other neuronal cell types in the CNS[4]. Experiments using simultaneous recordings from the soma and axon have provided direct evidence for this proposal[5–11], with recent studies in cortical layer 5 pyramidal neurons indicating that the site of action potential initiation lies at the distal end of the axon initial segment (AIS)[12,13].

Why action potentials are initiated in the axon is still unclear. Early theoretical studies proposed that this is the case because the density of Na^+ channels in the AIS is high[14,15]. Consistent with this idea, simulations using morphologically realistic models of cortical pyramidal neurons required a high Na^+ channel density in the AIS to replicate experimental findings from cortical neurons[16,17]. In addition to these theoretical studies, antibody staining for Na^+ channels and associated proteins indicates that the Na^+ channel density in the AIS is high in many neuronal types[11,18–24]. By contrast, cell-attached and outside-out patch-clamp studies indicate that there are similar densities of Na^+ channels in the AIS and soma[7,25]. These electrophysiological estimates led to the idea that rather than Na^+ channel density, unique gating properties of Na^+ channels could underlie action potential generation. Consistent with this, it has been proposed that action potential generation in the axon can be explained by the more hyperpolarized voltage-dependence of activation of Na^+ channels in the AIS[25].

Here we describe studies of the distribution and properties of Na^+ channels in the AIS of cortical layer 5 pyramidal neurons. We conclude that the density of Na^+ channels in the AIS is high (on average ~50-fold higher than the density at the soma and proximal dendrites), and that it has been underestimated in patch studies owing to tight anchoring of Na^+ channels to the actin cytoskeleton. In addition, using morphologically realistic models we find that a high AIS Na^+ channel density (~2,500 pS μm^{-2}) is required to account for experimental observations on the rate of rise of axonal action potentials, as well as on action potential initiation and backpropagation.

RESULTS

Patch experiments

We first attempted directly to assess the density of voltage-activated Na^+ channels in the AIS of cortical layer 5 pyramidal neurons using cell-attached patch-clamp recordings (**Fig. 1a**). We recorded fast, transient inward Na^+ currents in patches from the AIS ($n = 43$ from 35 neurons) up to the onset of myelination (~50 μm from the axon hillock; range: 35–52 μm) and compared these to Na^+ currents recorded at the soma ($n = 19$) under similar conditions (**Fig. 1b**). The Na^+ peak current in the AIS was similar to that observed at the soma, although there was a slight trend for larger Na^+ currents at more distal locations in the AIS (**Fig. 1b**; slope of linear fit 0.08 pA μm^{-1}, $n = 62$). Similar observations were made using outside-out patch-clamp recordings (data not shown). These data are consistent with previous observations in hippocampal subicular neurons using

[1]Division of Neuroscience, John Curtin School of Medical Research, Australian National University, Garran Road, Canberra ACT 0200, Australia. [2]Medical Research Council, Laboratory of Molecular Biology, Hills Road, Cambridge CB2 0QH, UK. [3]School of Kinesiology, Simon Fraser University, 8888 University Drive, Vancouver, British Columbia V5A 1S6, Canada. [4]Present address: Brain Research Institute, University of Zürich, Winterthurerstrasse 190, CH-8057 Zürich, Switzerland. Correspondence should be addressed to G.J.S. (greg.stuart@anu.edu.au).

Received 15 October 2007; accepted 17 December 2007; published online 20 January 2008; doi:10.1038/nn2040

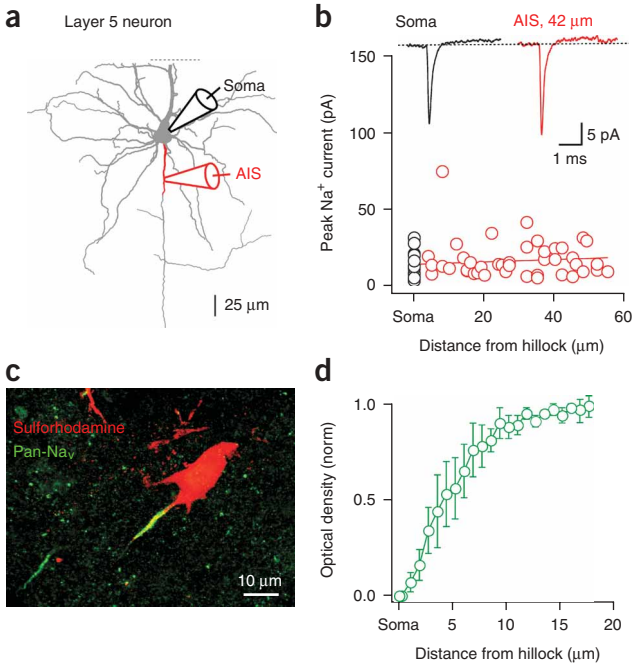

Figure 1 Divergence of AIS Na^+ channel density estimates using cell-attached recording and Na^+ channel antibody staining. (**a**) Schematic of the cell-attached recording configuration showing the location of somatic (black) and AIS recording pipettes (red). (**b**) Plot of peak Na^+ current in cell-attached patches from the soma (black) and in the AIS (red; $n = 62$, 46 neurons) at different distances from the axon hillock. Red line, linear fit to the data (slope, 0.08 pA μm^{-1}). Inset, examples of Na^+ currents at the soma and distal AIS activated by step depolarizations to ~0 mV (75 mV positive to the resting potential) preceded by pre-pulses (100 ms duration) to ~−100 mV (25 mV negative to the resting potential). (**c**) Confocal image of a layer 5 pyramidal neuron filled with a red dye (Sulforhodamine 101) using a whole-cell recording pipette and subsequently stained using a pan-alpha Na^+ channel antibody labeled with a green fluorescent tag (Alexa 488). (**d**) Plot of optical density of sodium channel antibody staining against distance from the axon hillock ($n = 4$). Optical density (green line) was base-lined at the axon hillock, normalized to the maximum in the AIS, and averaged (± s.e.m.) between different neurons.

cell-attached patch-clamp recordings[7], and with recent outside-out recordings from cortical layer 5 pyramidal neurons[25].

Antibody experiments

The finding that the Na^+ channel density in the AIS is only marginally higher than at the soma is puzzling. Modeling studies indicate that to replicate experimental observations on axonal action potential initiation the density of Na^+ channels in the AIS needs to be at least an order of magnitude higher than at the soma[14–17] (but see ref. 25). Furthermore, a number of immunocytochemical studies have shown that the intensity of Na^+ channel staining in the AIS in many neuronal cell types is significantly higher than at the soma or in internodal regions[11,18–24]. To assess and localize Na^+ channel staining in cortical layer 5 pyramidal neurons, we filled individual neurons with a red fluorescent dye (Sulforhodamine 101) through the whole-cell recording pipette before staining them with a pan-alpha antibody against Na^+ channels (**Fig. 1c**). These experiments indicated that there was intense Na^+ channel antibody labeling in the AIS region of layer 5 pyramidal neurons, with no observable staining of the somatic or proximal dendritic membrane. Na^+ channel staining in the AIS reached a maximum within 10 µm from the axon hillock, and was then constant over the region of the AIS examined (**Fig. 1d**).

Can slow inactivation of Na^+ channels explain the paradox?

These data indicate a discrepancy between the patch experiments and the antibody staining. One possible explanation for this is that the Na^+ channel density in the AIS is high, as observed in the antibody experiments, but that these channels are not available owing to slow inactivation[26]. To determine whether this was the case, we tested the impact of increasing the pre-pulse duration on the peak Na^+ current observed in patches from the AIS (**Supplementary Fig. 1** online). Increasing the pre-pulse duration did not lead to an increase in peak Na^+ current, indicating that slow inactivation cannot explain the observed difference in AIS Na^+ channel density between the results of patch and antibody experiments.

Whole-cell voltage-clamp experiments

Although the patch experiments described above provide arguably the best available quantitative method for assessing functional Na^+ channel

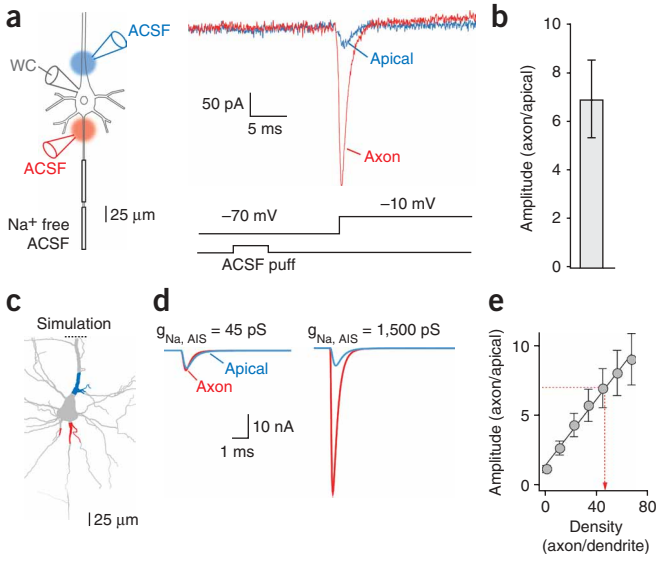

Figure 2 Comparison of AIS and proximal apical dendritic whole-cell Na^+ current indicates a high Na^+ channel density in the AIS. (**a**) Left, schematic diagram of the recording configuration in Na^+-free ACSF showing the location of the two ACSF application pipettes for applying Na^+-rich ACSF to the apical dendrite (blue) and AIS (red), and the somatic whole-cell recording pipette. Right, examples of whole-cell Na^+ current evoked by voltage steps (middle), which were preceded by brief (5 ms) applications (bottom) of Na^+-rich ACSF to the AIS ('axon', red) or the proximal apical dendrite ('apical', blue). (**b**) Average (± s.e.m.) ratio of AIS to proximal dendritic Na^+ current measured using somatic whole-cell recording. (**c**) Morphology used in simulations for selective activation of Na^+ channels in the proximal apical dendrites (blue) or AIS, including some basal dendrites (red). (**d**) Examples of somatic whole-cell Na^+ current obtained from the indicated membrane regions using an AIS Na^+ channel density ($g_{Na,\,AIS}$) of 45 pS μm^{-2} (left) or 1,500 pS μm^{-2} (right). (**e**) Ratio of AIS to proximal dendritic somatic Na^+ current versus the ratio of axonal to dendritic Na^+ channel density in simulations with different AIS Na^+ channel densities. Mean from three models with different morphologies (± s.e.m.). Data fitted with a linear function $y = 0.12x + 1.4$. The experimentally determined ratio (6.9) requires an axonal Na^+ channel density ~45 times greater than in the proximal dendrites (red dotted line).

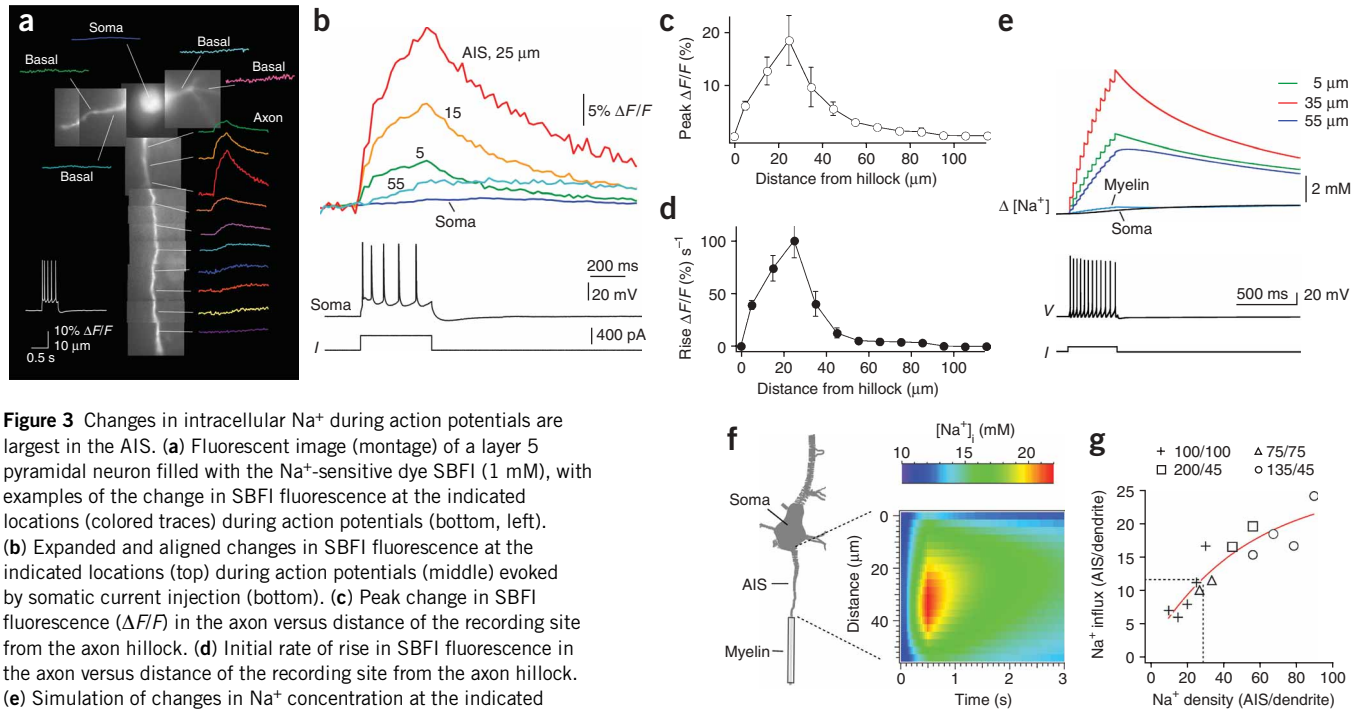

Figure 3 Changes in intracellular Na^+ during action potentials are largest in the AIS. (**a**) Fluorescent image (montage) of a layer 5 pyramidal neuron filled with the Na^+-sensitive dye SBFI (1 mM), with examples of the change in SBFI fluorescence at the indicated locations (colored traces) during action potentials (bottom, left). (**b**) Expanded and aligned changes in SBFI fluorescence at the indicated locations (top) during action potentials (middle) evoked by somatic current injection (bottom). (**c**) Peak change in SBFI fluorescence ($\Delta F/F$) in the axon versus distance of the recording site from the axon hillock. (**d**) Initial rate of rise in SBFI fluorescence in the axon versus distance of the recording site from the axon hillock. (**e**) Simulation of changes in Na^+ concentration at the indicated locations (top) during action potentials (middle) evoked by somatic current injection (bottom). Note the similarity with **b**. (**f**) Na^+ concentration (color coded) in the AIS versus both distance from hillock and time. (**g**) Ratio of the change in Na^+ concentration (normalized to baseline) in the AIS divided by that in the proximal basal dendrites in models with different AIS-to-proximal basal Na^+ channel densities. Models with the indicated somatic-to-dendritic Na^+ channel density (in pS μm^{-2}) were used (different symbols). The experimentally determined AIS-to-basal dendrite ($\Delta F/F$) ratio ($\sim$12) requires an axonal Na^+ channel density $\sim$30 times that in the proximal dendrites (dotted line).

density, given the contrasting results from the antibody studies we were concerned they might have underestimated the Na^+ channel density. We therefore designed a method for assessing Na^+ channel density in different regions of the neuron while recording in the whole-cell configuration (**Fig. 2a**). In these experiments, we bathed neurons in a Na^+-free solution and then puffed normal Na^+-rich extracellular solution (ACSF) alternatively onto the AIS and the proximal apical dendrites ($\sim$50 μm from the soma). Depolarizing voltage steps from –70 mV to –10 mV, administered through the somatic whole-cell recording pipette, were used to activate voltage-gated Na^+ channels. To minimize diffusion of ACSF away from the location of the puffer pipette, we applied Na^+-rich ACSF for brief periods (5 ms) just before the onset of voltage steps (**Fig. 2a**). These experiments revealed that the somatic whole-cell Na^+ current was significantly larger during application of Na^+-rich ACSF to the AIS than during similar applications to the proximal apical dendrites. Within individual cells, the application of Na^+-rich ACSF to the AIS led to somatic Na^+ currents that were on average 6.9 ± 1.6 times those observed after the application of Na^+-rich ACSF to the proximal apical dendrites of the same neurons (**Fig. 2b**; $n = 7$; $P < 0.01$).

We used computer simulations to determine whether these data can be explained by a difference in Na^+ channel density in the dendrites and the AIS. These simulations included Na^+ channel models based on experimentally determined gating properties of somatic and AIS Na^+ channels (**Supplementary Fig. 2** online). We simulated local application of Na^+-rich ACSF by including Na^+ channels in all segments (both axonal and dendritic) within a circular area (diameter $\sim$30 μm) centered on the AIS or proximal apical dendrite (**Fig. 2c**; red and blue segments, respectively). When the Na^+ channel density was uniform (45 pS μm^{-2}) at both locations, the somatic whole-cell Na^+ currents had similar amplitudes (**Fig. 2d**, left; AIS/apical = 1.1). We obtained larger somatic Na^+ currents during simulation of local applications of Na^+-rich ACSF to the AIS only if the Na^+ channel density in the AIS was substantially increased. For example, an AIS Na^+ channel density of 1,500 pS μm^{-2}, with a uniform somato-dendritic dendritic density of 45 pS μm^{-2}, led to 8.3-fold larger somatic Na^+ currents (**Fig. 2c,d**, right). To rule out bias we averaged the relative increase in AIS compared to proximal apical Na^+ current (AIS/apical) in models with three different morphologies and plotted this against the AIS Na^+ channel density (**Fig. 2e**, $n = 3$). Using the experimentally obtained peak amplitude ratio of 6.9, we estimate that the Na^+ channel density in the AIS is approximately 45 times that in the proximal dendrites (**Fig. 2e**, red line).

Sodium imaging experiments

We next used Na^+ imaging to investigate Na^+ channel activation in the AIS. We filled layer 5 neurons with the Na^+-sensitive dye SBFI (1 mM) and imaged changes in intracellular Na^+ during action potential trains evoked by somatic current injection (**Fig. 3a**). Consistent with earlier work in cerebellar Purkinje neurons[27], changes in SBFI fluorescence during action potentials were largest in the axon (**Fig. 3a–c**), with the greatest change occurring in the middle of the AIS, approximately 25 μm from the soma (**Fig. 3c**). This site also corresponds to the location where changes in fluorescence had the fastest initial rate of rise (**Fig. 3d**), indicating that the AIS represents the primary site of Na^+ influx during action potential trains, and that changes in fluorescence at more proximal and distal axonal locations are due to diffusion of Na^+ from this site. We found little if any fluorescence change at the soma or in apical or basal dendrites (**Fig. 3a,b**). Comparison of the SBFI signal in the AIS 25 μm from the soma with that in basal dendrites

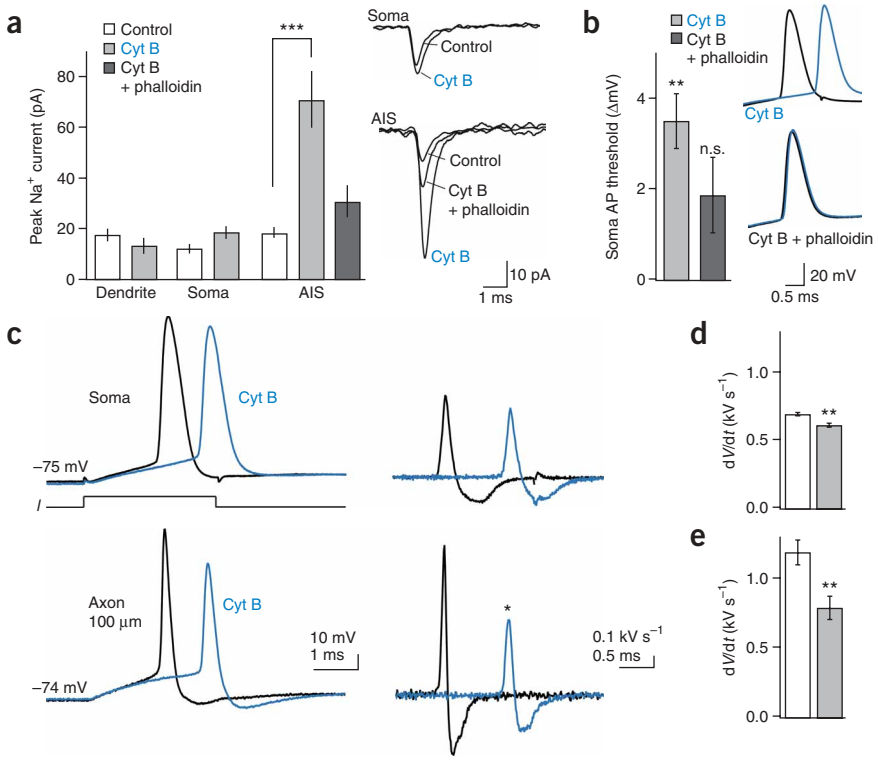

Figure 4 The actin cytoskeleton influences AIS Na^+ channel density and action potential properties. (**a**) Left, peak Na^+ current evoked by steps to 0 mV in cell-attached recordings from the distal AIS (>30 μm from the soma), soma and apical dendrite (5–140 μm from the soma) under control conditions (open bars), 25 min after intracellular application of cytochalasin B (Cyt B; 20 μM, gray bars), and 25 min after co-application of Cyt B and phalloidin (50 μM, dark gray bars). Right, example Na^+ currents recorded at the soma (top) or AIS in the indicated conditions (average of 8–20 sweeps). (**b**) Left, bar plot of the change in somatic action potential threshold after application of Cyt B (20 μM, gray) and after application of Cyt B with phalloidin (50 μM, dark gray). Right, examples of action potentials recorded at the soma under the indicated conditions. (**c**) Left, somatic (top) and axonal action potentials (bottom; 100 μm from the hillock) recorded before (black) and after (blue) perfusion with Cyt B (30 μM). Action potentials evoked by a 2 nA current injection at the soma (middle). Right, first derivative of the somatic (top) and axonal (bottom) action potential in control (black) and Cyt B (blue). Note the significant reduction in rate-of-rise of axonal action potential in Cyt B (asterisk). (**d**,**e**) Bar plots of somatic (**d**) and axonal (**e**) action potential rate-of-rise in control (open) and after Cyt B (filled; $P < 0.001$, $n = 7$).

at a similar distance from the soma indicated that the change in fluorescence in the AIS was approximately 12-fold larger than in proximal basal dendrites (axon: 18.5 ± 4.7% $\Delta F/F$, $n = 3$, compared to basal dendrites: 1.5 ± 0.8% $\Delta F/F$, $n = 4$). This difference cannot be accounted for by differences in surface to volume ratio, as the diameter of proximal basal dendrites is similar to that of the AIS (**Supplementary Fig. 3** online). Identical results to those described above with SBFI were obtained using the Na^+-sensitive fluorescent dye sodium green ($n = 8$; data not shown).

We performed computer simulations of the Na^+ influx to determine whether the observed changes in Na^+ concentration were consistent with a high density of Na^+ channels in the AIS. Similar to experimental data, models with a high Na^+ channel density in the AIS (3,000 pS μm^{-2}) had the largest Na^+ influx in the middle of the AIS, with smaller and slower rises in Na^+ at more proximal and distal axonal sites (**Fig. 3e**; compare with **Fig. 3b**). We observed only very small increases in Na^+ at the soma and myelinated axonal regions (**Fig. 3e**). To obtain more detailed insights into the space- and time-dependent changes in Na^+ influx we plotted Na^+ concentration during a train of action potentials against both time and space in the AIS (**Fig. 3f**). This analysis shows that the largest Na^+ influx occurs in the AIS 20–40 μm from the axon hillock. These simulations (**Fig. 3e**,**f**) using a high AIS Na^+ channel density closely mimicked the experimentally observed changes in SBFI fluorescence (**Fig. 3a–d**).

We next quantified the Na^+ channel density that was required to mimic the observed 12-fold larger $\Delta F/F$ in the AIS compared to the proximal basal dendrites. As the dendritic Na^+ channel density in the basal dendrites is unknown, we used cell-attached recordings to assess the Na^+ channel density in the proximal basal dendrites (6–35 μm from the soma; $n = 5$). These experiments indicated that the apparent Na^+ channel density in the proximal basal dendrites is low and similar to that observed at the soma (**Supplementary Fig. 3**). We next varied the density of Na^+ channels in the AIS while maintaining a constant low density of Na^+ channels in all dendritic compartments, and determined the relationship between the change in Na^+ concentration (divided by the baseline) in the AIS and that in the proximal basal dendrites (**Fig. 3g**). To obtain repetitive firing in these models we needed to increase the somatic and/or dendritic Na^+ channel density above previous estimates[5]. Similar to the simulations used to mimic the whole-cell voltage-clamp data (**Fig. 2e**), we found that the experimentally observed 12-fold larger $\Delta F/F$ in the AIS compared to that seen in the proximal basal dendrites required an AIS Na^+ channel density that was approximately 30-fold higher than that in the proximal basal dendrites (**Fig. 3g**). This conclusion was robust for a range of somatic and dendritic Na^+ channel density combinations (**Fig. 3g**).

Role of the cytoskeleton

The antibody, whole-cell voltage-clamp and Na^+ imaging experiments described above provide evidence that patch-clamp recordings significantly underestimate the Na^+ channel density in the AIS (by 30–45-fold). As voltage-activated Na^+ channels are known to interact with the actin cytoskeleton by binding to Ankyrin G[19], which is localized to the AIS[20], we hypothesized that this discrepancy can be explained if anchoring of Na^+ channels to the cytoskeleton prevents them being drawn into the tip of the patch pipette. To test this theory we depolymerized actin filaments using either latrunculin B or cytochalasin B, which increase Na^+ channel mobility in the AIS[28]. We made whole-cell recordings from the soma of layer 5 neurons using a pipette solution that included latrunculin B or cytochalasin B (20 μM; Sigma-Aldrich). After allowing ~25 min for diffusion into the neuron, we began cell-attached recordings. In some cases we obtained cell-attached recordings from the same axonal site (±5 μm) before and after depolymerization of actin filaments. Internal perfusion of layer 5 pyramidal neuron somata with actin depolymerizing agents significantly increased the amplitude of Na^+ currents recorded in the AIS

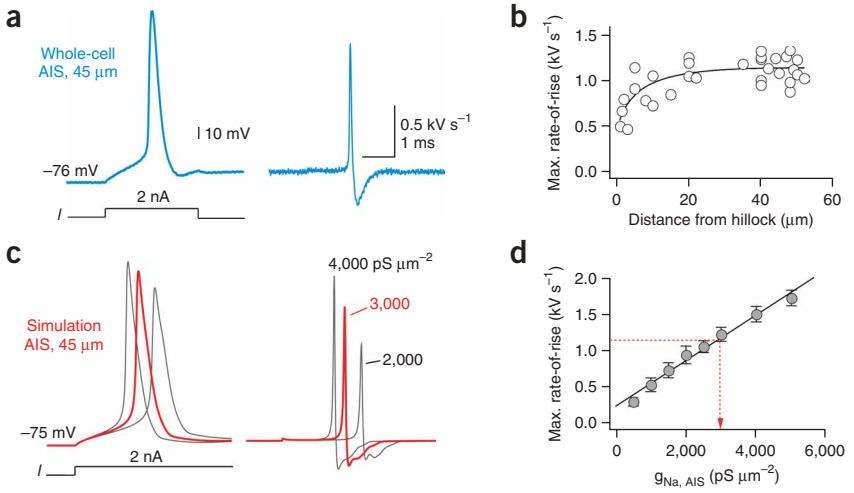

Figure 5 Simulation of axonal action potential rate-of-rise requires a high Na^+ channel density in the AIS. (**a**) Left, example of an axonal action potential recorded in the AIS (45 μm from the hillock, blue), evoked by a 2-nA current injected into the soma (bottom). Right, first derivative of action potential voltage. (**b**) Axonal action potential rate-of-rise versus distance from the axon hillock. Data fitted with a logarithmic function. (**c**) Axonal action potentials (left) and the first derivative of action potential voltage (right) recorded in the AIS (45 μm from the axon hillock) in models with the indicated AIS Na^+ channel densities. (**d**) Plot of AIS Na^+ channel density ($g_{Na,\ AIS}$) versus axonal action potential rate-of-rise (45 μm from the axon hillock). Average from three models with different morphologies (± s.e.m.). Data fitted with a linear regression ($y = 0.0003x + 0.23$). Dotted line (red) shows the AIS Na^+ channel density (~3,000 pS μm^{-2}) required to reproduce an action potential rate-of-rise of 1.13 kV s^{-1} (the experimental average in the distal AIS).

(**Fig. 4a**). On average, the peak Na^+ current recorded in cell-attached patches from the distal AIS increased threefold (**Fig. 4a**; control: 19 ± 2.5 pA ($n = 20$) versus depolymerization: 57 ± 8.6 pA ($n = 14$); $P < 0.001$). This increase in peak Na^+ current in the AIS was not due to a change in the voltage-dependence of activation or inactivation (**Supplementary Table 1** online), and was blocked when the actin stabilizer phalloidin (50 μM) was applied with cytochalasin B in the whole-cell recording solution (**Fig. 4a**; $n = 12$; $P < 0.05$). Actin depolymerization did not change the amplitude of Na^+ currents in cell-attached patches from either the soma ($n = 5$) or proximal apical dendrites (**Fig. 4a**; 5–140 μm from the soma, $n = 4$; $P > 0.05$). Together, these results show that disruption of the actin cytoskeleton leads to larger Na^+ currents in patch recordings selectively from the AIS. We interpret these data as indicating that anchoring of voltage-activated Na^+ channels to the actin cytoskeleton inhibits their detection in patch-clamp recordings from the AIS. Presumably this is because Na^+ channels are physically prevented from being drawn into the tip of the patch pipette during formation of the membrane seal, analogous to the findings of Milton and Caldwell at the neuromuscular junction[29].

Previous work indicates that disruption of the actin cytoskeleton increases the mobility of Na^+ channels in the AIS[28], which is likely to lead to redistribution of Na^+ channels to sites distant from the AIS. Given that the AIS is the site of action potential initiation in layer 5 pyramidal neurons[12,13], Na^+ channel redistribution away from this site would be expected to alter action potential properties. We therefore analyzed action potentials evoked by brief somatic current injections (3 ms; 2–3 nA) immediately after establishing the whole-cell recording configuration using pipettes with cytochalasin B, and compared them with those recorded after 25 min (**Fig. 4b**). Disruption of the actin cytoskeleton did not influence somatic action potential peak amplitude or half-width ($P > 0.05$; data not shown; $n = 7$). However, analysis of somatic action potential threshold indicated that depolymerization of the actin cytoskeleton significantly depolarized the action potential threshold by 4.3 ± 0.6 mV (**Fig. 4b**; $n = 7$; $P < 0.016$), and this effect was blocked by inclusion of the actin stabilizer phalloidin (50 μM) with cytochalasin B in the whole-cell recording solution (**Fig. 4b**; $n = 8$; $P > 0.08$). The rheobase current threshold for action potentials was also increased from 325 ± 42 pA to 533 ± 66 pA ($n = 6$; $P < 0.001$). Similar results were obtained with latrunculin B ($n = 8$; data not shown). These findings are analogous to those obtained in mice lacking cerebellar Ankyrin-G, where loss of Na^+ channel clustering at the AIS of Purkinje neurons leads to an increase in the rheobase current needed to initiate action potentials[19], and are consistent with the idea that disruption of the actin cytoskeleton causes Na^+ channels to move away from the AIS, thereby raising the action potential threshold.

To investigate the effect of disruption of the actin cytoskeleton on axonal action potential properties, we made simultaneous whole-cell recordings from the soma and proximal axon blebs[13] (110 ± 9 μm from the hillock; $n = 7$). In these experiments, both whole-cell recording pipettes contained 30–60 μM cytochalasin B and action potentials were triggered by 2-nA step current injections at the soma. These experiments revealed that disruption of the actin cytoskeleton leads to a small ~9% change in somatic action potential rate-of-rise (**Fig. 4c,d**; control: 686 ± 11 V s^{-1} versus cytochalasin B: 607 ± 14 V s^{-1}) but a much larger ~33% reduction in the rate-of-rise of axonal action potentials (**Fig. 4c,e**; control: 1,186 ± 83 V s^{-1} versus cytochalasin B: 783 ± 76 V s^{-1}; $P < 0.05$). As the action potential rate-of-rise (dV/dt) is directly related to the local Na^+ channel density ($dV/dt = I_{Na}/C_{local}$; where I_{Na} is the current flowing through Na^+ channels and C_{local} is the 'local' membrane capacitance), these data provide additional evidence that disruption of the actin cytoskeleton leads to the movement of Na^+ channels away from the AIS.

Simulating axonal action potential rate-of-rise

What Na^+ channel density is required in the AIS to reproduce experimental observations on axonal action potential rate-of-rise? We quantified axonal action potential rate-of-rise in whole-cell recordings at different sites along the AIS (**Fig. 5a,b**). These experiments indicated that axonal action potential rate-of-rise increases logarithmically with distance from the axon hillock (**Fig. 5b**). On average, the axonal action potential rate-of-rise was 791 ± 67 V s^{-1} in the proximal AIS (1–15 μm from the hillock; $n = 10$) compared to 1,131 ± 32 V s^{-1} in the distal AIS (35–52 μm from the hillock, $n = 17$). We next generated models with different AIS Na^+ channel densities to see what AIS density is required to best fit the experimental data on axonal action potential rate-of-rise (**Fig. 5c**). Action potentials in these simulations were evoked by somatic current injections and were recorded in the distal AIS, 45 μm from the soma. These results, based on models with three different morphologies, show that the rate-of-rise of action potentials in the distal AIS scales approximately linearly with the AIS Na^+ channel density, with an AIS Na^+ channel density of ~3,000 pS μm^{-2} required to generate action

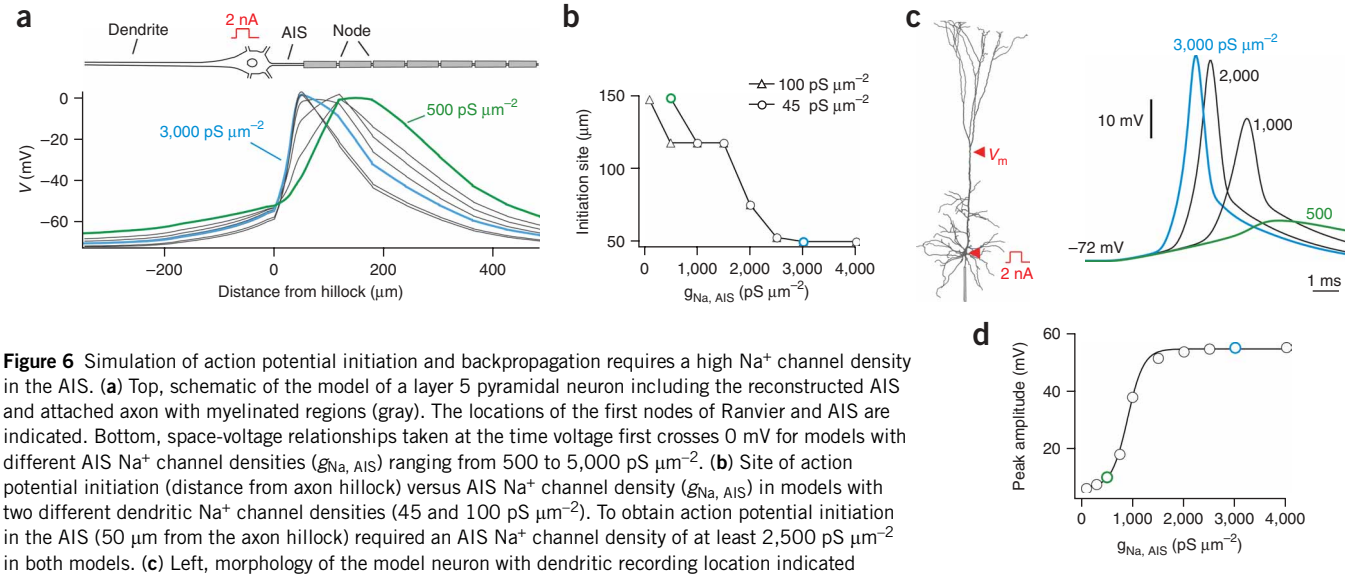

Figure 6 Simulation of action potential initiation and backpropagation requires a high Na^+ channel density in the AIS. (**a**) Top, schematic of the model of a layer 5 pyramidal neuron including the reconstructed AIS and attached axon with myelinated regions (gray). The locations of the first nodes of Ranvier and AIS are indicated. Bottom, space-voltage relationships taken at the time voltage first crosses 0 mV for models with different AIS Na^+ channel densities ($g_{Na,\ AIS}$) ranging from 500 to 5,000 pS μm^{-2}. (**b**) Site of action potential initiation (distance from axon hillock) versus AIS Na^+ channel density ($g_{Na,\ AIS}$) in models with two different dendritic Na^+ channel densities (45 and 100 pS μm^{-2}). To obtain action potential initiation in the AIS (50 µm from the axon hillock) required an AIS Na^+ channel density of at least 2,500 pS μm^{-2} in both models. (**c**) Left, morphology of the model neuron with dendritic recording location indicated (V_m, 495 µm from the soma). Right, examples of action potentials recorded in the apical dendrite 495 µm from the soma in models with the indicated AIS Na^+ channel densities. (**d**) Dendritic action potential amplitude (495 µm from the soma) versus AIS Na^+ channel density ($g_{Na,\ AIS}$). Data fit with a sigmoid function with half-maximum density ~1,000 pS μm^{-2}.

potentials with a rate-of-rise similar to that observed experimentally (**Fig. 5d**, red line; compare with **Fig. 5b**). This is ~60 times the somato-dendritic Na^+ channel density in pyramidal neurons (~50 pS μm^{-2})[5,30].

Simulating action potential initiation and backpropagation

We next performed simulations to investigate the dependence of the site of action potential initiation on the Na^+ channel density in the AIS. Recent studies in layer 5 pyramidal neurons indicate that action potentials in these neurons are initiated in the distal AIS[12,13]. **Figure 6a** shows overlayed space-voltage plots in simulations in which the AIS Na^+ channel density was increased from 500 to 5,000 pS μm^{-2}, while maintaining a fixed somato-dendritic Na^+ density of 45 pS μm^{-2} and a nodal density of 2,500 pS μm^{-2}. We defined the site of action potential initiation as the location where the voltage first crossed 0 mV and plotted this against the Na^+ channel density in the AIS (**Fig. 6b**). Action potentials in these models were initiated at the first or second nodes of Ranvier when the AIS Na^+ channel density was low (100–1,500 pS μm^{-2}), with action potential initiation only occurring in the distal AIS (as observed experimentally) when the density of Na^+ channels in the AIS was greater than ~2,500 pS μm^{-2} (**Fig. 6b**); a value ~50 times the somato-dendritic Na^+ channel density in pyramidal neurons (~50 pS μm^{-2})[5,30]. This finding was robust for the two somato-dendritic Na^+ channel densities investigated in these simulations (**Fig. 6b**).

Finally, we investigated the dependence of action potential backpropagation on the density of Na^+ channels in the AIS (**Fig. 6c**). Dendritic action potential amplitude depended steeply on the density of Na^+ channels in the AIS, with a clear threshold around 1,000 pS μm^{-2} (**Fig. 6d**). Dendritic action potential amplitude did not approach experimentally observed values of 55 mV[5] until the density of Na^+ channels in the AIS was greater than ~2,000 pS μm^{-2} (**Fig. 6d**), 40 times the somato-dendritic Na^+ channel density in pyramidal neurons (~50 pS μm^{-2})[5,30].

These simulations support the results of the experiments using antibody staining, whole-cell voltage-clamp and Na^+ imaging by showing that experimental observations on the axonal properties, initiation, and dendritic backpropagation of action potentials can be observed only in models where the density of Na^+ channels in the AIS is substantially higher than that found in the soma and proximal dendrites of layer 5 pyramidal neurons. Taking the estimates from the experiments and modeling together, we conclude that the Na^+ channel density in the AIS is on average ~50 times that observed in the soma and proximal dendrites. Assuming a somato-dendritic Na^+ channel density of 50 pS μm^{-2} in pyramidal neurons[5,30], in absolute terms this equates to an AIS Na^+ channel density of ~2,500 pS μm^{-2}.

DISCUSSION

In this paper we provide new evidence in support of the long-held view that the density of voltage-activated Na^+ channels in the AIS is significantly higher than that found at the soma and proximal dendrites. This prediction has been questioned by patch-clamp recordings from the AIS, which have suggested that the density of Na^+ channels in the AIS is similar to[7] or only slightly higher than that found at the soma[25]. However, evidence from immunocytochemistry, whole-cell voltage-clamp and Na^+ imaging studies contradicted this observation. This paradox can be accounted for by anchoring of Na^+ channels in the AIS to the actin cytoskeleton, restricting their ability to be drawn into the patch-pipette tip during cell-attached and outside-out recordings. Consistent with this idea we observed an increase in the apparent density of Na^+ channels selectively in patches from the AIS following disruption of the actin cytoskeleton (**Fig. 4**). Finally, we show in morphologically realistic models that experimental observations on axonal action potential rate-of-rise, as well as initiation and backpropagation, require high AIS Na^+ channel densities (on the order of ~2,500 pS μm^{-2}).

Comparisons with previous studies

The notion that the density of Na^+ channels in the AIS is significantly higher than in the soma and dendrites dates back to the original work on action potential initiation in spinal motoneurons, where it was observed that the threshold for the so-called 'initial segment' spike was significantly more hyperpolarized than the threshold for the

'somato-dendritic' spike[1–3]. Theoretical studies have suggested that this difference in threshold is best explained by a high density of Na^+ channels in the AIS[14–17], consistent with our experimental observations using immunocytochemistry (**Fig. 1c,d**), whole-cell voltage-clamp (**Fig. 2**) and Na^+ imaging (**Fig. 3**), and also with our simulations (**Figs. 5** and **6**).

Previous patch estimates of the Na^+ channel density in AIS have concluded that it is similar to that at the soma[7,25] (**Fig. 1b**), and it has been argued that a negative shift in the voltage-dependence of activation of AIS Na^+ channels in the absence of a high AIS Na^+ channel density can explain axonal action potential initiation in cortical pyramidal neurons[25]. This notion was not supported by our simulations (**Fig. 6**). Experimental observations on the site of action potential initiation in layer 5 pyramidal neurons[12,13] could only be accounted for in models where the AIS Na^+ channel density was significantly ($\sim$50 times) higher than the somato-dendritic Na^+ channel density, despite using Na^+ channel models in the AIS and nodes of Ranvier with the observed more negative voltage-dependence (**Supplementary Fig. 2** online). A similar conclusion was drawn from an earlier simulation study[17].

Our model-based estimates of the difference in channel density between the AIS and the somato-dendritic compartment line up well with our experimental estimates. Our comparison of whole-cell Na^+ currents during local application of Na^+-rich solution to the AIS and the proximal apical dendrites could only be explained if the Na^+ channel density at the AIS was $\sim$45 times that at proximal apical dendritic sites (**Fig. 2e**), whereas the change in local Na^+ concentration in the AIS compared to that in the proximal basal dendrites during action potential trains required the Na^+ channel density at the AIS to be $\sim$30 times that in the proximal basal dendrites (**Fig. 3g**). Together with the estimates from our simulations (**Figs. 5** and **6**), these results lead us to conclude that the AIS Na^+ channel density is $\sim$50-fold greater than that observed in the soma and proximal dendrites of cortical layer 5 pyramidal neurons. Interestingly, this difference is similar to previous estimates of the high Na^+ channel density in nodal compared to internodal regions of mammalian axons[31].

Molecular identity of Na^+ channels in the AIS

Consistent with a previous study[25], we observed a hyperpolarized shift ($\sim$10 mV) in the voltage-dependence of activation of AIS Na^+ channels, although in our experiments this was found throughout the entire AIS (not shown), and was associated with a similar shift ($\sim$6 mV) in the voltage-dependence of inactivation (**Supplementary Fig. 2** and **Supplementary Table 1**). Recent work indicates that in the mature nervous system the Na^+ channel isoform $Na_v1.6$ is localized to the AIS and nodes of Ranvier, whereas $Na_v1.2$ is found primarily in unmyelinated axons[22,32,33]. Electrophysiological characterization of these two Na^+ channel isoforms indicates that the voltage-dependence of activation and inactivation of $Na_v1.6$ is shifted by 10–15 mV to more negative potentials compared to that of $Na_v1.2$ (ref. 34). This finding agrees with our observed negative shift in the voltage-dependence of activation and inactivation of Na^+ channels in the AIS compared to the soma, and suggests that the molecular identity of AIS Na^+ channels in layer 5 pyramidal neurons is likely to be $Na_v1.6$, whereas somato-dendritic Na^+ channels are likely to include $Na_v1.2$, possibly with $Na_v1.1$ and 1.3 (ref. 35).

Anchoring of sodium channels to the AIS

The first electron micrographs of the AIS of pyramidal neurons in the cortex indicated that it contains an electron-dense coating similar to that observed at nodes of Ranvier[36]. More recent studies show that the AIS can act as a diffusion barrier for certain membrane proteins, by tethering them to the actin cytoskeleton[28,37]. Voltage-activated Na^+ channels interact with the membrane-bound protein Ankyrin G[19] as well as with ßIV spectrin[21], and targeting of Na^+ channels to the AIS is thought to involve an Ankyrin G-binding motif located in the cytoplasmic linker between domains II and III of the α-subunit of voltage-activated Na^+ channels[38]. This molecular interaction is important for anchoring Na^+ channels to the actin cytoskeleton in the AIS[39]. Consistent with the idea that Na^+ channels in the AIS are bound tightly to the actin cytoskeleton, the apparent Na^+ channel density in cell-attached recordings from the AIS, but not the soma or dendrites, was significantly increased following disruption of the actin cytoskeleton (**Fig. 4a**). These data support the hypothesis that patch-clamp estimates of AIS Na^+ channel density[7,25] (**Fig. 1b**) underestimate the true density as Na^+ channels anchored to the actin cytoskeleton are prevented from being drawn into the patch membrane during seal formation, as has been described at the neuromuscular junction[29]. The tight physical coupling between the cytoskeleton and voltage-gated Na^+ channels observed here might be unique to Na^+ channels, as recent findings indicate that the high density of Kv1 channels in the distal AIS seen with immunocytchemisty[23] is also observed in cell-attached recordings[13].

Following disruption of the actin cytoskeleton, patch estimates of Na^+ channel density in the AIS were only three- to fourfold higher than in the soma and proximal dendrites (**Fig. 4a**). These new estimates based on patch-clamp recordings are substantially lower than the estimates of the Na^+ channel density in the AIS from antibody staining (**Fig. 1c,d**), whole-cell recording (**Fig. 2**), Na^+ imaging (**Fig. 3**) and modeling (**Figs. 5** and **6**). This is likely to be the case for two reasons. First, after disruption of the actin cytoskeleton, lateral diffusion of Na^+ channels away from the AIS[28,37] will reduce the AIS Na^+ channel density. Indeed, breakdown of the actin cytoskeleton was associated with a reduction in axonal action potential rate-of-rise (**Fig. 4e**), consistent with loss of approximately one-third of the Na^+ channels from the AIS (**Fig. 5d**). Second, it is likely that disruption of the actin cytoskeleton in our experiments is incomplete, such that a significant proportion of the Na^+ channels in the AIS are still tightly anchored to the cytoskeleton after treatment with latrunculin or cytochalasin.

Role of Na^+ channels in the AIS

One of the advantages of a high AIS Na^+ channel density is that it forces action potential initiation to occur in a localized region of the neuron, the distal AIS (**Fig. 6**), providing a single site where inputs can influence action potential output. If the AIS Na^+ channel density is reduced, action potential initiation shifts to the nodes of Ranvier, the next available site with high Na^+ channel density (**Fig. 6a,b**). Our simulations indicate that the first node of Ranvier is electrotonically too far from the soma to support invasion by backpropagating action potentials when the AIS Na^+ channel density is low (**Fig. 6c,d**). Thus, an important functional role of the high AIS Na^+ channel density is to compensate for the large electrical load imposed by the soma, enabling axonal action potentials to invade the soma and backpropagate into the dendritic tree. In addition, reducing the AIS Na^+ channel density moves the site of action potential initiation away from the known locus of inhibitory input that specifically targets the AIS[40], which presumably exerts a powerful influence on the initiation and backpropagation of action potentials. The high AIS Na^+ channel density is also likely to be important for the precise timing of action potentials in response to synaptic input[41]. In conclusion, we show that a high Na^+ channel density in the AIS, maintained by tight anchoring to the actin cytoskeleton, provides neurons with a unique site for the integration of synaptic input as well as a mechanism for signaling neuronal output back to the synapse.

METHODS

General. Wistar rats (2–4 weeks old) were anesthetized by inhalation of isoflurane and decapitated, and sagittal brain slices (300 μm) of somatosensory cortex were prepared according to guidelines approved by the Animal Ethics Committee of the Australian National University and the University of Freiburg (Germany). During recording, slices were superfused with oxygenated (95% O_2, 5% CO_2) extracellular solution (ACSF) containing (in mM): 125 NaCl, 3 KCl, 1.25 NaH_2PO_4, 25 $NaHCO_3$, 25 glucose, 2 $CaCl_2$, 1 $MgCl_2$ (pH 7.4) at 32–34 °C, unless otherwise stated. Patch-pipette recordings were obtained from the soma, the proximal dendrites or the first ~50 μm of unmyelinated AIS of large cortical layer 5 pyramidal neurons using standard methods[42]. In some cases recordings were made from axon blebs[13]. Current and voltage were low-pass filtered at 2 kHz and 10 kHz, respectively, and sampled at 20–50 kHz using an ITC-18 interface (Instrutech) controlled by an Apple PowerPC running Axograph software (Molecular Devices). Data are presented as mean ± s.e.m. Statistical analysis between two independent datasets was performed using a two-tailed unpaired Student's *t*-test. For multiple group comparisons we used a one-way analysis of variance (ANOVA) followed by Bonferroni post-test using Prism 4.0 (GraphPad Software). The level of significance for rejecting the null hypothesis was set to 0.05.

Patch recordings. Cell-attached recordings were made using pipettes of similar resistance (11–15 MΩ) with a patch-clamp amplifier (Axopatch 200B, Molecular Devices). No differences in the degree or time of suction applied to the back of pipettes was required to form high resistance (3–10 GΩ) seals at somatic or axonal sites, suggesting that similar membrane areas were sampled. For cell-attached recordings, we filled pipettes with the following solution (in mM): 125 NaCl; 30 TEA; 5 4-AP; 2 $CaCl_2$; 1 $MgCl_2$; 0.2 $CdCl_2$; 10 HEPES (290 mOsm, pH 7.2 with NaOH). Steady-state inactivation was assessed using 100-ms prepulses between –100 mV and –10 mV before stepping to a test pulse of 0 mV. Steady-state activation was assessed using 100-ms prepulses to –100 mV followed by test pulses to voltages between –80 mV and +10 mV. Peak current was converted to conductance assuming a reversal potential of +55 mV, normalized to the maximum, and data fitted with a single Bolzmann function. The resting membrane potential of the soma and AIS were assumed to be –75 mV after junction potential correction[13]. Currents were leak subtracted on-line (P/5) with Axograph software.

Immunocytochemistry. Immunohistological identification of Na^+ channels was performed with a pan-alpha anti-sodium channel antibody (SP20; provided by W. Catterall, University of Washington). Layer 5 pyramidal neurons were labeled intracellularly during somatic whole-cell recordings using patch-pipettes containing the red fluorescent dye Sulforhodamine (101; Invitrogen). Slices were fixed with PLP (4% paraformaldehyde, 0.2% periodate and 1.2% lysine in 0.1 M in phosphate buffer), re-sliced at 8–30 μm thickness using a cryostat, and incubated with the pan-alpha anti-sodium channel antibody for 48–72 h before detection with an Alexa-coupled anti-rabbit antibody (Alexa Fluor 488; Invitrogen) using confocal microscopy. As an alternative to labeling with Sulforhodamine, in some cases slices were counterstained with propidium iodide to stain the nuclei of layer 5 pyramidal neurons before incubation with anti-sodium channel antibody.

Somatic voltage-clamp. Somatic whole-cell voltage-clamp recordings were made with a patch-clamp amplifier (Axopatch 200B) using pipettes (3–5 MΩ) filled with the following solution (in mM): 135 mM CsCl, 4 mM $MgCl_2$, 10 mM EGTA, 4 mM Na_2ATP, 10 mM Na_2-phophosphocreatine, 10 mM HEPES (pH 7.2 with CsOH). During whole-cell voltage-clamp experiments, series resistance (5–10 MΩ) was compensated by greater than 85% (<5 μS lag). Brief voltage steps (–70 to –10 mV) were used to evoke Na^+ currents, and the external solution switched to one with zero Na^+ of the following composition (in mM): 140 NMDG, 3 mM KCl, 10 HEPES, 25 glucose, 2 $CaCl_2$, 1 $MgCl_2$ (pH 7.4 with HCl, oxygenated with 95% O_2/5% CO_2). In some cases this solution also included TTX (1 μM). Following almost complete block of inward Na^+ current (reduced to less than 5%), brief applications (10 ms) of standard Na^+-rich ACSF were applied alternatively to the AIS or proximal apical dendrite using standard patch pipettes filled with ASCF and controlled by two independent Picospritzers (General Valve). ACSF-filled application pipettes (5 MΩ) were positioned within 5 μm of the AIS (30 μm from the soma) and proximal apical dendrite (~50 μm from the soma), and ACSF was applied 10 ms before somatic voltage steps to ensure evoked Na^+ current was generated close to the pipette tip. Applications of ACSF were bracketed by somatic voltage steps alone, and the Na^+ current evoked during application of Na^+-containing extracellular solution to each location was determined by subtraction of the response to somatic voltage steps alone. To improve the temporal fidelity of somatic voltage-clamp these experiments were performed at room temperature (~23 °C).

Sodium imaging. During experiments using sodium-sensitive fluorescent dyes, pipettes (~5 MΩ) were tip filled with K-Gluconate whole-cell pipette solution without dye and back filled with the same K-Gluconate solution containing 1 mM SBFI (Invitrogen), or 1 mM Sodium Green (Invitrogen) dissolved in 150 mM KCl. Changes in fluorescence were acquired using a back-illuminated CCD camera (Red Shirt Imaging), analyzed with Neuroplex software (Red Shirt Imaging), and expressed as the change in fluorescence from baseline (F) divided by the baseline fluorescence (F) after subtraction of background fluorescence from a nearby region. Changes in fluorescence were investigated in small regions of interest (~10 μm in length). Imaging experiments were performed at room temperature (~23 °C).

Current clamp. Somatic and axonal whole-cell current-clamp recordings were made with current clamp amplifiers (BVC-700, Dagan Corp.) using pipettes (~5 MΩ) filled with a solution containing (in mM): 140 K-Gluconate, 2 $MgCl_2$, 2 Na_2ATP, 0.3 NaGTP, 10 HEPES (pH 7.2 with KOH). Action potentials were evoked by somatic current injection and membrane potential corrected for an estimated junction potential of approximately +12 mV. Action potential rate-of-rise was determined from the derivative of the membrane potential (dV/dt), with threshold defined as the membrane potential at which dV/dt equals 50 V s^{-1}.

Modeling. Computer simulations used Neurolucida reconstructions of layer 5 pyramidal neurons (**Fig. 6c**) imported into NEURON (v5.8)[43]. The morphology included the reconstructed AIS. At the end of the AIS we attached cylindrical sections of alternating length and diameter representing myelinated internodes (length: 60 μm; diameter: 1.6 μm) and nodes of Ranvier (length: 1 μm; diameter: 1.1 μm) with a total axonal length of 2.7 mm. On average, the location of the first node was ~110 μm from the axon hillock, consistent with previous studies[12,44]. The passive electrical properties R_m, C_m and R_i were set to 15,000 Ω cm^2, 0.9 μF cm^{-2} and 100 Ω cm, respectively, uniformly throughout all compartments. Myelination was simulated by reducing C_m to 0.02 μF cm^{-2}, which provided an axonal conduction velocity of 2.9 ms^{-1}, similar to that observed experimentally[13]. Nodal sections possessed a 400-fold increased resting conductance. Spines were modeled by doubling C_m and halving R_m in spiny dendritic sections. The resting membrane potential at the soma was set to –75 mV. All simulations were run with 5-μs time steps (unless otherwise noted) and the nominal temperature of simulations was 37 °C.

The voltage-dependence of activation and inactivation of a Hodgkin-Huxley based Na^+ channel model[16] was set to the experimentally observed values (**Supplementary Table 1** and **Supplementary Fig. 2**). The Na^+ equilibrium potential was set to +55 mV. The action potential threshold at the soma was set to –60 mV. Unless otherwise stated the Na^+ channel density was 45 pS μm^{-2} in the dendrites and soma, 2,500 pS μm^{-2} in nodes of Ranvier, and 80 pS μm^{-2} in internodal myelinated sections[45]. The density of Na^+ channels in the AIS was varied from 45 to 5,000 pS μm^{-2}, was uniform over the first 45 μm, and then decreased linearly in the distal AIS[24]. Na^+ channel models based on allosteric gating or non-sigmoid activation kinetics[46,47] were tested but did not adequately reproduce action potential kinetics.

For **Fig. 3** the internal Na^+ concentration was modeled with a previously described mechanism for Na^+ diffusion and a Na^+/K^+ exchanging pump[48]. Pump distribution was 12 μA cm^{-2} and Na^+ diffusion was set to 0.6 μm^2 ms^{-1} in all compartments. The resting Na^+ concentration was set to 10 mM. Simulation time steps were increased to 100 μs and data were analyzed using IGOR 4.08 (Wavemetrics).

The model included a high-voltage-activated K^+ channel (Kv)[16], a faster low-voltage activated Kv1-like K^+ channel ('Kv1'), as described[49], and a

slowly-activating and non-inactivating M-type K^+ channel ('Km')[16]. Potassium channel densities were adjusted to obtain fast action potential repolarization and large amplitude afterhyperpolarizations in the distal AIS[13]. The density of Kv, Kv1 and Km were set to 20, 100 and 5 pS μm^{-2}, respectively, in the soma, dendrites and inter-nodal sections, and increased linearly with distance from the axon hillock in the AIS to 2,000 pS μm^{-2} in the distal AIS and nodes for Kv and Kv1, and to 50 pS μm^{-2} for Km. The K^+ reversal potential was set to –85 mV. I_h channels were included in the soma and dendrites with an exponential increase in density with distance from the soma, and kinetics and voltage dependence as described previously[50]. I_h channels were not included in the axon.

Note: Supplementary information is available on the Nature Neuroscience website.

ACKNOWLEDGMENTS

We thank W. Catterall for the gift of the pan-alpha sodium channel antibody. This work was supported by the Alexander von Humboldt Foundation (G.J.S.) and a NRSA Senior Fellowship (P.C.R.).

AUTHOR CONTRIBUTIONS

M.H.P.K. performed the patch and whole-cell current-clamp experiments, as well as simulations, and wrote the paper; S.U.I. performed the antibody experiments; B.M.K. helped with the sodium imaging experiments and performed the associated simulations; S.R.W. and P.C.R. helped with the patch experiments; and G.J.S. performed the whole-cell voltage-clamp and sodium imaging experiments and wrote the paper.

Published online at http://www.nature.com/natureneuroscience
Reprints and permissions information is available online at http://npg.nature.com/reprintsandpermissions

1. Coombs, J.S., Curtis, D.R. & Eccles, J.C. The generation of impulses in motoneurones. *J. Physiol. (Lond.)* **139**, 232–249 (1957).
2. Fatt, P. Sequence of events in synaptic activation of a motoneurone. *J. Neurophysiol.* **20**, 61–80 (1957).
3. Fuortes, M.G.F., Frank, K. & Becker, M.C. Steps in the production of motoneuron spikes. *J. Gen. Physiol.* **40**, 735–752 (1957).
4. Eccles, J.C. *The Physiology of Synapses* (Springer, Berlin, 1964).
5. Stuart, G.J. & Sakmann, B. Active propagation of somatic action potentials into neocortical pyramidal cell dendrites. *Nature* **367**, 69–72 (1994).
6. Stuart, G. & Hausser, M. Initiation and spread of sodium action potentials in cerebellar Purkinje cells. *Neuron* **13**, 703–712 (1994).
7. Colbert, C.M. & Johnston, D. Axonal action-potential initiation and Na^+ channel densities in the soma and axon initial segment of subicular pyramidal neurons. *J. Neurosci.* **16**, 6676–6686 (1996).
8. Stuart, G., Schiller, J. & Sakmann, B. Action potential initiation and propagation in rat neocortical pyramidal neurons. *J. Physiol. (Lond.)* **505**, 617–632 (1997).
9. Clark, B.A., Monsivais, P., Branco, T., London, M. & Hausser, M. The site of action potential initiation in cerebellar Purkinje neurons. *Nat. Neurosci.* **8**, 137–139 (2005).
10. Shu, Y., Duque, A., Yu, Y., Haider, B. & McCormick, D.A. Properties of action-potential initiation in neocortical pyramidal cells: evidence from whole-cell axon recordings. *J. Neurophysiol.* **97**, 746–760 (2007).
11. Meeks, J.P. & Mennerick, S. Action potential initiation and propagation in CA3 pyramidal axons. *J. Neurophysiol.* **97**, 3460–3472 (2007).
12. Palmer, L.M. & Stuart, G.J. Site of action potential initiation in layer 5 pyramidal neurons. *J. Neurosci.* **26**, 1854–1863 (2006).
13. Kole, M.H.P., Letzkus, J.J. & Stuart, G.J. Axon initial segment Kv1 channels control axonal action potential waveform and synaptic efficacy. *Neuron* **55**, 633–647 (2007).
14. Dodge, F.A. & Cooley, J.W. Action potential of the motoneuron. *IBM J. Res. Develop.* **17**, 219–229 (1973).
15. Moore, J.W., Stockbridge, N. & Westerfield, M. On the site of impulse initiation in a neurone. *J. Physiol. (Lond.)* **336**, 301–311 (1983).
16. Mainen, Z.F., Joerges, J., Huguenard, J.R. & Sejnowski, T.J. A model of spike initiation in neocortical pyramidal neurons. *Neuron* **15**, 1427–1439 (1995).
17. Rapp, M., Yarom, Y. & Segev, I. Modeling back propagating action potential in weakly excitable dendrites of neocortical pyramidal cells. *Proc. Natl. Acad. Sci. USA* **93**, 11985–11990 (1996).
18. Wollner, D.A. & Catterall, W.A. Localization of sodium channels in axon hillocks and initial segments of retinal ganglion cells. *Proc. Natl. Acad. Sci. USA* **83**, 8424–8428 (1986).
19. Zhou, D. *et al.* AnkyrinG is required for clustering of voltage-gated Na channels at axon initial segments and for normal action potential firing. *J. Cell Biol.* **143**, 1295–1304 (1998).
20. Kordeli, E., Lambert, S. & Bennett, V. AnkyrinG. A new ankyrin gene with neural-specific isoforms localized at the axonal initial segment and node of Ranvier. *J. Biol. Chem.* **270**, 2352–2359 (1995).
21. Komada, M. & Soriano, P. ßIV-spectrin regulates sodium channel clustering through ankyrin-G at axon initial segments and nodes of Ranvier. *J. Cell Biol.* **156**, 337–348 (2002).
22. Boiko, T. *et al.* Functional specialization of the axon initial segment by isoform-specific sodium channel targeting. *J. Neurosci.* **23**, 2306–2313 (2003).
23. Inda, M.C., DeFelipe, J. & Munoz, A. Voltage-gated ion channels in the axon initial segment of human cortical pyramidal cells and their relationship with chandelier cells. *Proc. Natl. Acad. Sci. USA* **103**, 2920–2925 (2006).
24. Van Wart, A., Trimmer, J.S. & Matthews, G. Polarized distribution of ion channels within microdomains of the axon initial segment. *J. Comp. Neurol.* **500**, 339–352 (2007).
25. Colbert, C.M. & Pan, E. Ion channel properties underlying axonal action potential initiation in pyramidal neurons. *Nat. Neurosci.* **5**, 533–538 (2002).
26. Ulbricht, W. Sodium channel inactivation: molecular determinants and modulation. *Physiol. Rev.* **85**, 1271–1301 (2005).
27. Lasser-Ross, N. & Ross, W.N. Imaging voltage and synaptically activated sodium transients in cerebellar Purkinje cells. *Proc. Biol. Sci.* **247**, 35–39 (1992).
28. Nakada, C. *et al.* Accumulation of anchored proteins forms membrane diffusion barriers during neuronal polarization. *Nat. Cell Biol.* **5**, 626–632 (2003).
29. Milton, R.L. & Caldwell, J.H. Na current in membrane blebs: implications for channel mobility and patch clamp recording. *J. Neurosci.* **10**, 885–893 (1990).
30. Magee, J.C. & Johnston, D. Characterization of single voltage-gated Na^+ and Ca^{2+} channels in apical dendrites of rat CA1 pyramidal neurons. *J. Physiol. (Lond.)* **487**, 67–90 (1995).
31. Shrager, P. Sodium channels in single demyelinated mammalian axons. *Brain Res.* **483**, 149–154 (1989).
32. Boiko, T. *et al.* Compact myelin dictates the differential targeting of two sodium channel isoforms in the same axon. *Neuron* **30**, 91–104 (2001).
33. Kaplan, M.R. *et al.* Differential control of clustering of the sodium channels Na(v)1.2 and Na(v)1.6 at developing CNS nodes of Ranvier. *Neuron* **30**, 105–119 (2001).
34. Rush, A.M., Dib-Hajj, S.D. & Waxman, S.G. Electrophysiological properties of two axonal sodium channels, Nav1.2 and Nav1.6, expressed in mouse spinal sensory neurones. *J. Physiol. (Lond.)* **564**, 803–815 (2005).
35. Komai, S. *et al.* Postsynaptic excitability is necessary for strengthening of cortical sensory responses during experience-dependent development. *Nat. Neurosci.* **9**, 1125–1133 (2006).
36. Peters, A., Proskauer, C.C. & Kaiserman-Abramof, I.R. The small pyramidal neuron of the rat cerebral cortex. The axon hillock and initial segment. *J. Cell Biol.* **39**, 604–619 (1968).
37. Winckler, B., Forscher, P. & Mellman, I. A diffusion barrier maintains distribution of membrane proteins in polarized neurons. *Nature* **397**, 698–701 (1999).
38. Garrido, J.J. *et al.* A targeting motif involved in sodium channel clustering at the axonal initial segment. *Science* **300**, 2091–2094 (2003).
39. Lai, H.C. & Jan, L.Y. The distribution and targeting of neuronal voltage-gated ion channels. *Nat. Rev. Neurosci.* **7**, 548–562 (2006).
40. Howard, A., Tamas, G. & Soltesz, I. Lighting the chandelier: new vistas for axo-axonic cells. *Trends Neurosci.* **28**, 310–316 (2005).
41. Kuba, H., Ishii, T.M. & Ohmori, H. Axonal site of spike initiation enhances auditory coincidence detection. *Nature* **444**, 1069–1072 (2006).
42. Stuart, G.J., Dodt, H.-U. & Sakmann, B. Patch-clamp recordings from the soma and dendrites of neurones in brain slices using infrared video microscopy. *Pflugers Arch.* **423**, 511–518 (1993).
43. Carnevale, N.T. & Hines, M.L. *The Neuron Book* (Cambridge University Press, Cambridge, 2006).
44. Sloper, J.J. & Powell, T.P. A study of the axon initial segment and proximal axon of neurons in the primate motor and somatic sensory cortices. *Phil. Trans. R. Soc. Lond. B* **285**, 173–197 (1979).
45. Neumcke, B. & Stämpfli, R. Sodium currents and sodium-current fluctuations in rat myelinated nerve fibres. *J. Physiol. (Lond.)* **329**, 163–184 (1982).
46. Baranauskas, G. & Martina, M. Sodium currents activate without a Hodgkin-and-Huxley-type delay in central mammalian neurons. *J. Neurosci.* **26**, 671–684 (2006).
47. Taddese, A. & Bean, B.P. Subthreshold sodium current from rapidly inactivating sodium channels drives spontaneous firing of tuberomammillary neurons. *Neuron* **33**, 587–600 (2002).
48. Canavier, C.C. Sodium dynamics underlying burst firing and putative mechanisms for the regulation of the firing pattern in midbrain dopamine neurons: a computational approach. *J. Comput. Neurosci.* **6**, 49–69 (1999).
49. Akemann, W. & Knopfel, T. Interaction of Kv3 potassium channels and resurgent sodium current influences the rate of spontaneous firing of Purkinje neurons. *J. Neurosci.* **26**, 4602–4612 (2006).
50. Kole, M.H.P., Hallermann, S. & Stuart, G.J. Single I_h channels in pyramidal neuron dendrites: properties, distribution, and impact on action potential output. *J. Neurosci.* **26**, 1677–1687 (2006).